Observation of wave-breaking-free square pulses in a fiber ring laser

Tonghui Liu (刘彤辉)[1], Dongfang Jia (贾东方)[1,*], Ying Liu (刘 迎)[1,2], Zhaoying Wang (王肇颖)[1], and Tianxin Yang (杨天新)[1]

[1]*Key Laboratory of Opto-electronic Information and Technical Science, College of Precision Instrument and Opto-electronics Engineering, Tianjin University, Tianjin 300072, China*

[2]*Department of Applied Physics, Tianjin University, Tianjin 300072, China*

**Corresponding author: jiadf@tju.edu.cn*

Received May 7, 2015; accepted August 19, 2015; posted online September 9, 2015

We experimentally and numerically demonstrate the generation of square pulses without any wave-breaking in a fiber ring laser. A segment of nonzero dispersion-shifted fiber is used to increase the laser cavity length and to optimize the parameters of the laser cavity. In the experiment, the pulse width can be tuned in a wide range from 13.5 to 119.5 ns without wave-breaking while the peak power remains almost constant. The maximum single-pulse energy is up to 65.58 nJ at a pump power of 508 mW. Numerical results are in good agreement with the experimental results. Numerical results also reveal the role of cavity length and nonlinearity in generating a square pulse without pulse breakup.

OCIS codes: 060.3510, 140.3560, 140.3600, 140.4050.

doi: 10.3788/COL201513.101401.

Pulsed fiber lasers have attracted a lot of research interest due to their wide applications in telecommunications, industrial processing, and biophotonics. Different types of lasers based on various mechanisms have been reported, such as stretched-pulse fiber lasers[1,2], self-similar fiber lasers[3,4], dissipative soliton fiber lasers[5], and so on. The dissipative soliton found in a system with both loss and gain features a rectangular shape in the spectrum and a Gaussian shape in the time domain, which provides a powerful way of generating high-energy pulses[6]. It was discovered later that, within a narrow range of laser parameters, a dissipative soliton mode-locked fiber laser could generate pulses with energy increasing linearly with the pump power without suffering pulse breakup. This kind of laser operates in the so-called dissipative soliton resonance (DSR) region[7–11] and possesses a rectangular temporal waveform and a Gaussian spectral shape[12]. On the other hand, Liu *et al.* reported that the difference in pulse energy between the two orthogonal polarization axes plays a key role in generating a wave-breaking-free pulse [13]. As this kind of soliton has the characteristic that the pulse energy would increase with the pump power without suffering a pulse breakup, it has recently been investigated extensively. Experimental investigations of square pulses have been reported in mode-locked fiber lasers based on the nonlinear polarization rotation (NPR)[8,9] and the nonlinear amplifying loop mirror (NALM) techniques[10,11].

It was confirmed by experiments that a quasi-rectangular pulse could be generated both in the normal dispersion and anomalous dispersion regions[8,14]. In addition, it was theoretically demonstrated that the pulse width broadened with the decrease of the dispersion coefficient D in the anomalous dispersion regime[15]. Specifically, Zhang *et al.* reported a square pulse with a tuning range from 10 to 1716 ns and proposed that the large nonlinearity and a long cavity would be of benefit for increasing the tuning range and producing a pulse with a high energy[16]. Recently, dark-square-pulse bunches and harmonic mode-locking (HML) of dark-square pulses, as well as bright pulses were simultaneously observed in a graphene-oxide saturable absorber (GOSA) passively mode-locked Yb-doped fiber laser[17]. Despite the tuning capability in the temporal domain, the variety in the wavelength and repetition rate has also been achieved in a passively mode-locked fiber laser. Lin *et al.* proposed a wavelength-tunable mode-locked fiber laser that has a tuning range of 38 nm, operating in the DSR region[18]. Very recently, distributed ultrafast (DUF) lasers were proposed, with a fundamental cavity frequency that is linearly changeable as a function of the pulse wavelength[19]. However, the spectrum of the DUF laser features a narrow bandwidth and several Kelly sidebands that limit the further enhancement of the pulse energy. The advantage of the DSR region makes it easy for a passively mode-locked fiber laser to generate pulses with high energy up to hundreds of nJ.

In this Letter, square-pulse generation based on a mode-locked fiber laser is achieved by the NPR technique. A segment of nonzero dispersion-shifted fiber (NZ-DSF) with the dispersion coefficient of ~2.25 ps/(nm·km) at 1550 nm wavelength is inserted into the cavity to increase the length and manage the dispersion of the laser cavity. The relatively low dispersion coefficient would be beneficial to the increase of nonlinear effects compared with the standard single-mode fiber (SMF). To confirm the experimental results, the square-pulse formation of the mode-locked fiber laser has also been simulated numerically. The experimental configuration of the wave-breaking-free

fiber laser is schematically presented in Fig. 1. A segment of erbium-doped fiber (EDF) with a length of 1.5 m and erbium ion absorption of 30 dB/m at 980 nm is pumped by a 980 nm laser diode with a maximum pump power of 508 mW through a 980/1550 nm wavelength-division multiplexer (WDM). A polarization-dependent isolator (PD-ISO) is inserted into the cavity to ensure unidirectional propogation and linear polarization of the light. Two intracavity polarization controllers (PCs) are used to adjust the polarization state of the light. An optical coupler with 10 % output is used as the output port. An ~2.1 km NZ-DSF with a dispersion coefficient of 2.25 ps/(nm · km) is inserted into the cavity to increase the cavity length. An oscilloscope (TDS500 MHz 3052C) together with a 3 GHz photodetector and an optical spectrum analyzer (Anritsu Ms9740A) are used to monitor the trace, temporal profile, and the optical spectrum of the square pulse, respectively.

The fiber laser is mode-locked by the NPR technique. In our experiment, when the pump power is increased to a threshold of 180 mW, stable mode-locked square pulses are obtained. The status of mode-locking can be maintained while reducing the pump power to about 105 mW due to the pump power hysteresis effect. By increasing the pump power to the maximum of 508 mW, the width of the square wave reaches 119.5 ns. Figure 2(a) shows the profile of a single pulse that exhibits a square profile without other fine internal structure. The slowly decreasing top and the microstructure at the trailing edge are due to the response of our measurement system. The optical spectrum with a resolution of 0.03 nm at a pump power of 508 mW is shown in Fig. 2(b). The central wavelength and 3 dB bandwidth are 1562 and 6.97 nm, respectively.

The pedestal of the optical spectrum at the shorter wavelength originates from the amplified spontaneous emission (ASE) of the EDF. Correspondingly, the radio frequency (RF) spectrum of the output square pulse is measured by a 26.5 GHz RF spectrum analyzer (Agilent N9010A) with a resolution bandwidth (RBW) of 5 Hz, as shown in Fig. 2(c). The fiber laser can be mode-locked at the fundamental repetition rate of 95.15 kHz, and the signal-to-noise ratio (SNR) is larger than 60 dB, which indicates that we have achieved a stable pulse mode-locking state.

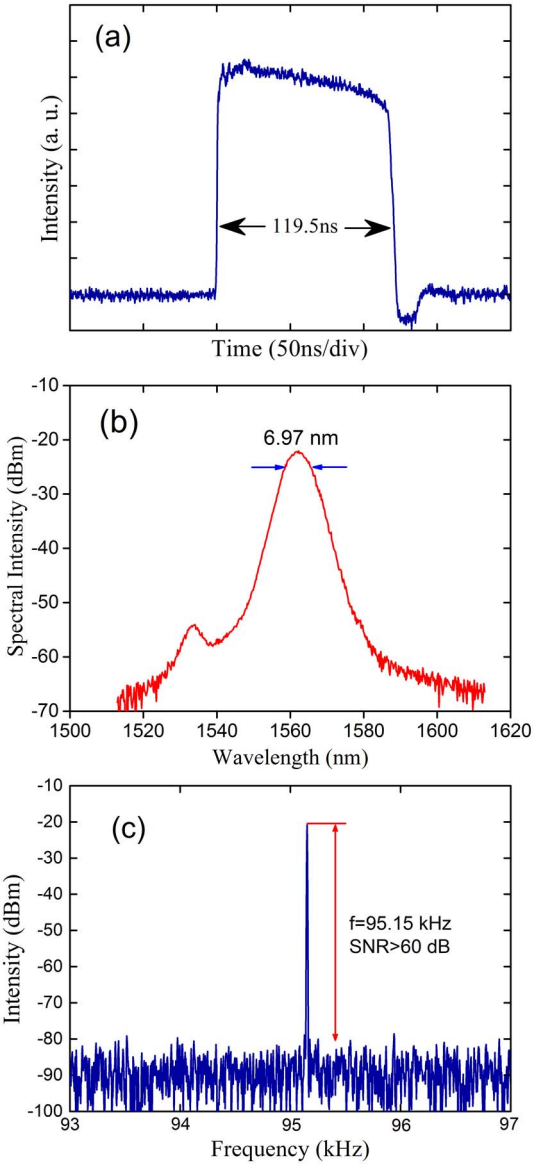

Fig. 2. (a) Profile of square pulse; (b) optical spectrum; (c) RF spectrum of the square pulse under a pump power of 508 mW.

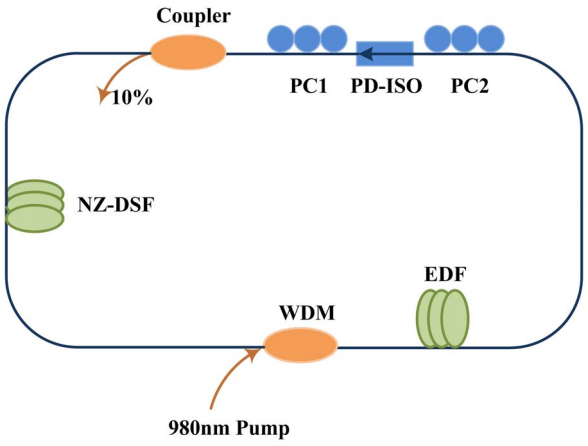

Fig. 1. Schematic of the experimental setup. OC, output coupler.

To further investigate the characteristics that the duration and the energy of the pulse will increase with the increasing pump power while the peak power of the pulse remains almost constant, the pulse evolution is recorded when the pump power is increased and the PCs are fixed in the experiment. As shown in Fig. 3, when the pump powers are tuned to 105, 218, 328, 455, and 508 mW, the pulse widths are measured to be 13.4, 62.9, 88.5, 108.3, and 119.5 ns, respectively. The wave-breaking-free pulses are observed without any multipulse oscillation and the pulse width broadens with the increase of the pump power.

The details of pulse widths and output powers versus the pump powers are shown in Fig. 4. The pulse width and the output power increase linearly with the pump

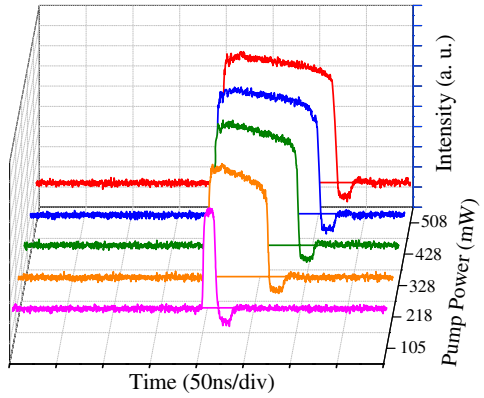

Fig. 3. Oscilloscope traces of square pulses under different pump powers.

power. When the pump power is enhanced from 105 to 508 mW, the pulse width increases from 13.4 to 119.5 ns and the output power increases from 0.39 to 6.24 mW. The maximum single-pulse energy is 65.58 nJ at a pump power of 508 mW.

The formation of the wave-breaking-free pulses in the laser is simulated numerically. The coupled Ginzburg–Landau equations (CGLEs) can be used to model the propagation of wave-breaking-free pulses in the weakly birefringent fibers[13,20]. The coupled equations are expressed by[21]

$$\frac{\partial u}{\partial z} = -i\beta u + \delta\frac{\partial u}{\partial t} - i\frac{\beta_2}{2}\frac{\partial^2 u}{\partial t^2} + i\gamma\left(|u|^2 + \frac{2}{3}|v|^2\right)u + \frac{i\gamma v^2 u^*}{3} + \frac{g-\alpha}{2}u + \frac{g}{2\Omega_g}\frac{\partial^2 u}{\partial t^2}, \tag{1a}$$

$$\frac{\partial v}{\partial z} = -i\beta v - \delta\frac{\partial v}{\partial t} - i\frac{\beta_2}{2}\frac{\partial^2 v}{\partial t^2} + i\gamma\left(|v|^2 + \frac{2}{3}|u|^2\right)v + \frac{i\gamma u^2 v^*}{3} + \frac{g-\alpha}{2}v + \frac{g}{2\Omega_g}\frac{\partial^2 v}{\partial t^2}, \tag{1b}$$

where u and v represent the slowly varying envelope of the pulse along two orthogonal polarization axes of the fiber; t and z denote the time and the propagation distance, respectively; $2\beta = 2\pi\Delta n/\lambda$ and $2\delta = 2\beta\lambda/2\pi c$ are the wavenumber difference of two modes and the inverse group velocity, respectively; α, β_2, γ, and Ω_g are the transmission loss coefficient of fiber, the fiber dispersion, the cubic refractive nonlinearity of the medium, and the bandwidth of the laser gain, respectively; g is the saturable gain of the EDF, described by $g = g_0\exp(-E_p/E_s)$ and g_0, E_p, and E_s are the small-signal gain coefficient, pulse energy, and gain saturation energy, respectively. The polarization additive pulse mode-locking (P-APM) element is combined by a polarizer provided by the PD-ISO and cavity birefringence, and the transmission function of passed pulses can be expressed as

$$T = \sin^2(\theta)\sin^2(\varphi) + \cos^2(\theta)\cos^2(\varphi) + 0.5\,\sin(2\theta)\sin(2\varphi)\cos(\phi_1 + \phi_2), \tag{2}$$

where θ and ϕ denote the angles between the polarization directions of the polarizer and the analyzer respective to the fast axis of the fiber, respectively; ϕ_1 is the phase delay caused by the PCs and ϕ_2 is the phase delay resulting from the fiber, including both the linear phase delay and the nonlinear phase delay.

The CGLEs mentioned above are solved with a standard split-step Fourier technique[22]. The following parameters are used in the simulations to match the experimental conditions: $\alpha = 0.2$ dB/km, $g_0 = 3\ \mathrm{m}^{-1}$, $\gamma = 4.5\ \mathrm{W}^{-1}\,\mathrm{km}^{-1}$ for EDF and $2.2\ \mathrm{W}^{-1}\,\mathrm{km}^{-1}$ for NZ-DSF, $\Omega_g = 30$ nm, $\beta_2 = 53\ \mathrm{ps}^2/\mathrm{km}$ for EDF and $-2.6\ \mathrm{ps}^2/\mathrm{km}$ for NZ-DSF. In our simulation, the lengths of NZ-DSF and EDF are chosen as 2145 and 1.5 m, respectively. The saturation energy E_s, which is proportional to the pump strength, is equal to 25 nJ. The angle θ is 0.25π and ϕ is 0.5π, while the phase delay ϕ_1 is 0.05π.

The dynamic evolution of the pulse is shown in Fig. 5(a). The length of the fiber and the nonlinearity are chosen to be 2145 m and $2.2\ \mathrm{W}^{-1}\,\mathrm{km}^{-1}$ for NZ-DSF, which are the same as that of the experimental setup. After a finite number of circulations, the original signal converges into a rectangular pulse without any pulse breakup. As shown by the green (middle pulse) line of Fig. 5(b), the pulse duration obtained after 1000 round trips is ~123 ns, which matches the experimental result. To investigate the influence of nonlinearity on the pulse width, we use SMFs with different nonlinear coefficients to form the laser cavity. It can be concluded that the pulse width is proportional to the nonlinearity of the cavity, being consistent with the experiments in Ref. [12]. It should be noted that the high pump power and long cavity are two factors in generating square pulses[23,24]. To further investigate the impact of cavity length on the pulse width, a number of different cavity lengths up to 2500 m are used in the simulation, as shown in Fig. 5(c). It is important to note that the cavity length is increased by a step size of 5 m, i.e., there may be appropriate parameters to generate square pulse other than integer ones. In addition, by changing some values, such as ϕ and E_s, different results could be obtained with the same cavity length. That is to say, by adjusting the PCs (or varying the value of ϕ in the

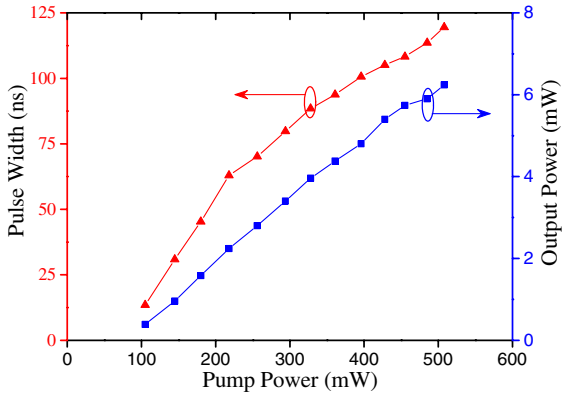

Fig. 4. Measured pulse widths and output powers versus pump powers.

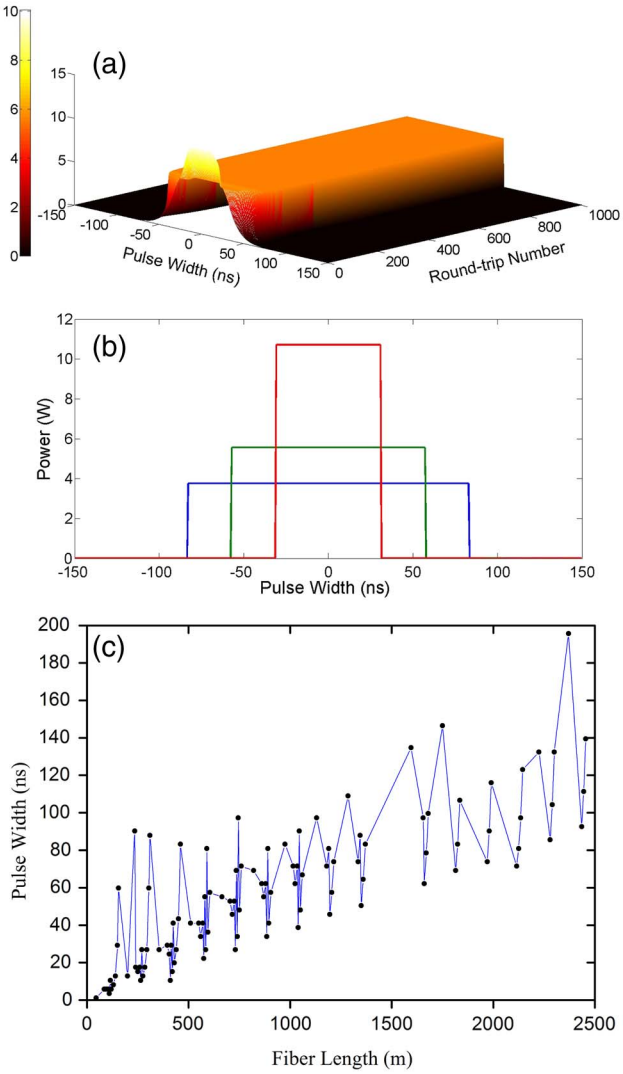

Fig. 5. Values used in the simulation of three figures are the same as the instruction of the passage except unless otherwise specified. (a) Dynamic evolution of wave-breaking-free pulses as a function of round-trip number; (b) pulse widths with different nonlinearity: red is $\gamma = 1.2\ \mathrm{W^{-1}\,km^{-1}}$, blue is $\gamma = 2.2\ \mathrm{W^{-1}\,km^{-1}}$, and green is $\gamma = 3.2\ \mathrm{W^{-1}\,km^{-1}}$; (c) dynamics of the pulse width at different cavity lengths. The dots represent the values of fiber length that enable the generation of square pulses.

simulation), or changing the pump power, different shapes of pulses may be generated as well as square pulses with various durations. At a certain value of fiber length, the pulse duration would vary within a limit by changing other parameters of the laser. The dots in Fig. 5(c) are nothing but the sampling points within a certain range. Nonetheless, the range under the condition of a long fiber length has a higher value compared with a short one. Therefore, in spite of the oscillation in Fig. 5(c), the pulse width tends to increase with the increase of the fiber length. The square pulse will not be generated until the cavity length is increased to approximately 45 m. With the increase of the cavity length, it becomes easier to generate a pulse with a rectangular shape. The broadest pulse of 195.7 ns is obtained at a length of 2370 m. It can be expected that the generation of broader square pulses is possible under the condition of a longer cavity.

In conclusion, wave-breaking-free square pulses generated in a mode-locked fiber laser based on the NPR technique are numerically and experimentally investigated. The stable square pulses are first generated through inserting a segment of NZ-DSF into the laser cavity. It is later demonstrated numerically that the nonlinearity and the length of the cavity play key roles in the generation of square pulses. Parameters should be chosen properly to generate square pulses.

This work was supported by the Natural Science Foundation of China (Nos. 61377078 and 61275084) and the National Basic Research Program of China (No. 2014CB340100).

References

1. H. Haus, K. Tamura, L. Nelson, and E. Ippen, IEEE J. Quantum Electron. **31**, 591 (1995).
2. C. Zhang, L. Chai, Y. Song, M. Hu, and C. Wang, Chin. Opt. Lett. **11**, 051403 (2013).
3. F. Ilday, J. Buckley, W. Clark, and F. Wise, Phys. Rev. Lett. **92**, 213902 (2004).
4. B. Oktem, C. Ülgüdür, and F. Ö. Ilday, Nat. Photonics **4**, 307 (2010).
5. A. Chong, W. H. Renninger, and F. W. Wise, Opt. Lett. **32**, 2408 (2007).
6. W. Tian, J. Zhu, Z. Wang, J. Wang, and Z. Wei, Chin. Opt. Lett. **12**, 031401 (2014).
7. D. J. Richardson, R. I. Laming, D. N. Payne, V. Matsas, and M. W. Phillips, Electron. Lett. **27**, 542 (1991).
8. L. Duan, X. Liu, D. Mao, L. Wang, and G. Wang, Opt. Express **20**, 265 (2012).
9. X. Li, S. Zhang, H. Zhang, M. Han, F. Wen, and Z. Yang, IEEE Photon. Tech. Lett. **26**, 2082 (2014).
10. S. K. Wang, Q. Y. Ning, A. P. Luo, Z. B. Lin, Z. C. Luo, and W. C. Xu, Opt. Express **21**, 2402 (2013).
11. J. H. Yang, C. Y. Guo, S. C. Ruan, D. Q. Ouyang, H. Q. Lin, Y. M. Wu, and R. H. Wen, IEEE Photon. J. **5**, 1500806 (2013).
12. X. Liu, Phys. Rev. A **81**, 023811 (2010).
13. X. Liu, Phys. Rev. A **82**, 053808 (2010).
14. X. Wu, D. Tang, H. Zhang, and L. Zhao, Opt. Express **17**, 5580 (2009).
15. P. Grelu, W. Chang, A. Ankiewicz, J. M. Soto-Crespo, and N. Akhmediev, J. Opt. Sci. Am. B **27**, 2336 (2010).
16. X. Zhang, C. Gu, G. Chen, B. Sun, L. Xu, A. Wang, and H. Ming, Opt. Lett. **37**, 1334 (2012).
17. R. Y. Lin, Y. G. Wang, P. G. Yan, G. L. Zhang, J. Q. Zhao, H. Q. Li, S. Q. Huang, G. Z. Cao, and J. A. Duan, IEEE Photon. J. **6**, 1 (2014).
18. H. Q. Lin, C. Y. Guo, S. C. Ruan, and J. H. Yang, Laser Phys. Lett. **11**, 085102 (2014).
19. X. Liu, Y. Cui, D. Han, X. Yao, and Z. Sun, Sci. Rep. **5**, 9101 (2015).
20. X. Liu, Phys. Rev. A **81**, 053819 (2010).
21. D. Mao, X. Liu, and H. Lu, Opt. Lett. **37**, 2619 (2012).
22. L. Zhao, D. Tang, H. Zhang, X. Wu, and N. Xiang, Opt. Express **16**, 9528 (2008).
23. G. Chen, C. Gu, L. Xu, H. Zheng, and H. Ming, Chin. Opt. Lett. **9**, 091405 (2011).
24. L. Liu, J. H. Liao, Q. Y. Ning, W. Yu, A. P. Luo, S. H. Xu, Z. C. Luo, Z. M. Yang, and W. C. Xu, Opt. Express **21**, 27087 (2013).